Materials Science-Poland, 40(1), 2022, pp. 9-24
http://www.materialsscience.pwr.wroc.pl/
DOI: 10.2478/msp-2022-0005

Effect of novel grain refiner and Ni alloying additions on microstructure and mechanical properties of Al-$Si_{9.8}$-$Cu_{3.4}$ HPDC castings – optimization using Multi Criteria Decision making approach

K. Ch Apparao[1,*], Praveen Kumar Bannaravuri[2], Kumar Swamy Pulisheru[3], E. D. Francis[4], Kalakanda Alfred Sunny[2], Gadudasu Babu Rao[2], P Freedon Daniel[5], Anil Kumar Birru[3]

[1]Department of Mechanical Engineering, Institute of Aeronautical Engineering, Hyderabad, India-500043

[2]Department of Mechanical Engineering, Karunya Institute of Technology and Sciences, Coimbatore-641114, India

[3]Department of Mechanical Engineering, National Institute of Technology, Manipur, India-795004

[4]Department of Mechanical Engineering, Wellfare Institute of Science, Technology and Management, Visakhapatnam-531173, India

[5]Department of Mechanical Engineering, SRM Institute of Science and Technology, NCR campus, Ghaziabad-201204, India

Studies dealing with process improvement of aluminum alloys and their grain structure refinement are the current area of interest in casting companies and foundries, the aim being to enhance the properties of the base metal. In this study, the microstructural and mechanical properties of commercial Al-$Si_{9.8}$-$Cu_{3.4}$ alloy die castings influenced by different additions of Al-3.5FeNb-1.5C master alloy (viz. 0 wt.%, 0.1 wt.%, and 1.0 wt.%) as a new grain refiner and Al-6Ni master alloy (viz. 0 wt.%, 0.5 wt.%, and 5.0 wt.%) as an alloying element have been investigated. A multi-criteria decision-making approach for the improvement of the die casting process was performed using grey relational analysis (GRA) and TOPSIS analytical techniques. It was observed that the primary aluminum α-grains were significantly refined, particularly at the lower addition level 0.1 wt.% of Al-3.5FeNb-1.5C, and conversely, poor grain refining efficiency was observed at a higher addition level 1.0 wt.% of Al-3.5FeNb-1.5C. Due to the refinement by Al-3.5FeNb-1.5C grain refiner and the effect of Ni alloying element additions, the ultimate tensile strength (UTS) and hardness (Brinell and micro) of the Al-$Si_{9.8}$-$Cu_{3.4}$ alloy are improved, particularly at 0.1 wt.% of Al-3.5FeNb-1.5C and 0.5 wt.% of Al-6Ni master alloys. Quantitatively, UTS, Brinell hardness, and microhardness values have been increased by 12.3%, 7.0%, and 20%, respectively.

Keywords: *die casting, Al–Si alloy, Al-3.5FeNb-1.5C grain refiner, Al-6Ni master alloy, GRA, TOPSIS, ultimate tensile strength and hardness*

1. Introduction

Nowadays, among the aluminum-based alloys, aluminum-silicon cast alloys are the most familiar choice of materials for the automotive industry to produce robust engineering parts due to their lightweight and high strength-to-weight ratio, which is one cause for the appreciable improvement in the overall fuel economy by optimal weighting [1, 2]. Mechanical properties of the aluminum-silicon alloys, in particular the tensile strength, ductility, hardness, and fatigue, are strongly dependent on the dendritic structure, and on primary Al α-grains in the respective microstructures [3, 4]. Kori et al. [5] observed that grain refinement is the most effective process to achieve homogeneously distributed small equiaxed grains, and in addition, following this process results in a high strength-to-weight ratio, excellent castability, and other desired properties [6–8].

Usually, the refinement of grains is carried out by introducing inoculating particles into the melt in the form of master alloys prepared by the Al-Ti-B ternary-based system [9–11]. Over the past 5 decades, 94%Al-5%Ti-1%B (Al-5Ti-1B) in par-

* E-mail: kchapparao@gmail.com

© K. Ch Apparao et al. 2022. This is an open access article distributed under the Creative Commons Attribution-NonCommercial-NoDerivatives 4.0 License. (http://creativecommons.org/licenses/by-nc-nd/4.0/)

ticular has been widely used as a common grain refiner, because Ti is one of the most common elements for the refinement of α-Al through heterogeneous nucleation [12–14]. But it fails to meet the expectations in the case of Al-Si cast alloys, where the silicon (Si) weight percent exceeds 4 wt.%, due to the formation of titanium silicides (i.e., TiSi, $TiSi_2$, and Ti_5Si_3), which cause an impairment of the grain refining efficiency of the master alloy by consuming the titanium content in the melt. This phenomenon is known as the poisoning effect [15–20].

To overcome this poisoning effect, various attempts were made; however, despite being numerous, none of these approaches is up to the mark, because they have failed to fully address this poisoning effect. But in recent studies, Nb-B novel grain refiner has been used to enhance the grain refinement performance in aluminum-silicon cast alloys; also, "it was concluded that the developed Al-1Nb-1B grain refiner can efficiently refine α-Al primary grains of binary Al-Si cast alloys due to the formation of Niobium borides which are more stable than Titanium borides" [21]. So, for this study, ferroniobium (FeNb) and carbon (C) based Al-3.5FeNb-1.5C master alloy has been attempted as a novel grain refiner for refinement of α-Al of Al-$Si_{9.8}$-$Cu_{3.4}$ alloy through heterogeneous nucleation [22]. Also, Al-Ni master alloy has been added at different weight percentages to the Al-$Si_{9.8}$-$Cu_{3.4}$ alloy to enhance the mechanical properties of the base alloy. Most of the recent studies in the literature look only into the effect of the alloying elements, taking them into consideration as a unique given process condition. Similarly, some other studies focus on the significance of casting process parameters without considering the diversity in the weight percentages of the alloying elements. In the present study, the first step was to ascertain the effects of Al-3.5FeNb-1.5C novel grain refiner, Ni alloying additions, and three prominently influencing high pressure die casting (HPDC) process parameters on tensile strength properties and hardness of Al-$Si_{9.8}$-$Cu_{3.4}$ cast alloy. In addition, optimization of these process parameters of die casting for obtaining higher tensile strength, hardness, and elongation has been studied using TOPSIS analysis as a multi-criteria decision-making approach in comparison with grey relational analysis (GRA) analysis [23–25]. The significant process parameter levels at which the best result occurs to a single response are considered as optimum levels.

2. Experimental design

For this research, the design of experiments has been prepared using the Taguchi approach. Identification of significant process parameters, which is the most important stage, is carried out based on the experimenter's experience, and is mainly based on this researcher's previous investigations into optimization of the die casting process [26]. Thus, based on insights gained from previous experimentation, this researcher has selected mainly three process parameters, viz. molten metal, die temperatures, and injection pressure, recognizing them as the most critical parameters in the experimental design. The other parameters were kept constant throughout the entire experiment. These parameters are designated as process parameters for the present investigation, along with Al-3.5FeNb-1.3C grain refiner and Al-6Ni alloying element as composition factors, to obtain optimal settings for the die casting parameters, in order to yield the optimum casting density by reducing the porosity of the Al-Si alloy castings. Taguchi provided a well-organized approach to estimate the optimal levels of significant input process parameters with the help of the L_{27} orthogonal array system. The selected levels for these input parameters are given in Table 1. Experimental designs for the fabrication of casting samples at different levels and weight percentages of parameters have been prepared with reference to the L_{27} orthogonal array.

3. Methodology

The details of the materials and processing methods that are used to fabricate the composite materials are discussed below.

Table 1. Process factors and their levels used in the experiments

Parameter destination	Input parameters	Parameter range	Level 1	Level 2	Level 3
A	Molten metal temperature (°C)	720–780	720	750	780
B	Al-3.5FeNb-1.5C (wt%)	0.0–0.1–1.0	0.0	0.1	1.0
C	Al-6Ni (wt%)	0.0–0.5–5.0	0.0	0.5	5.0
D	Die temperature (°C)	230–290	230	260	290
E	Injection pressure (MPa)	12–24	12	18	24

Table 2. Composition of Al-$Si_{9.8}$-$Cu_{3.4}$ alloy (wt.%) considered for this study

Al%	Si%	Cu%	Fe%	Ti%	Mg%	Ni%	Zn%	Pb%	Sn%	Mn%
86.18	9.839	3.474	0.189	0.184	0.041	0.008	0.008	0.043	0.013	0.007

Table 3. Input parameters and experimental values of output characteristics along with average porosity values for L_{27} orthogonal array

Expt. runs	Input factors					Output responses			Average
	A (°C)	B (wt.%)	C (wt.%)	D (°C)	E (MPa)	Tensile strength	Brinell hardness	Microhardness	porosity values
1	720	0	0	230	12	218.39	85	113	0.88
2	720	0	0.5	260	18	223.76	85	116	0.53
3	720	0	5	290	24	245.50	88	119	0.36
4	720	0.1	0	260	18	239.88	90	136	0.26
5	720	0.1	0.5	290	24	249.09	91	135	0.25
6	720	0.1	5	230	12	237.31	85	136	0.47
7	720	1	0	290	24	220.53	83	112	0.85
8	720	1	0.5	230	12	214.67	83	114	0.71
9	720	1	5	260	18	208.63	86	118	0.75
10	750	0	0	260	24	217.87	85	114	0.95
11	750	0	0.5	290	12	210.73	85	116	0.77
12	750	0	5	230	18	230.46	89	116	0.49
13	750	0.1	0	290	12	230.19	86	118	0.63
14	750	0.1	0.5	230	18	237.29	88	130	0.44
15	750	0.1	5	260	24	212.70	85	120	0.62
16	750	1	0	230	18	208.26	80	106	1.01
17	750	1	0.5	260	24	218.83	85	113	0.88
18	750	1	5	290	12	201.05	80	108	0.97
19	780	0	0	290	18	219.96	85	115	0.89
20	780	0	0.5	230	24	224.58	88	125	0.33
21	780	0	5	260	12	240.50	87	118	0.49
22	780	0.1	0	230	24	238.37	88	127	0.46
23	780	0.1	0.5	260	12	240.04	90	132	0.48
24	780	0.1	5	290	18	232.57	85	114	0.46
25	780	1	0	260	12	200.27	80	107	0.99
26	780	1	0.5	290	18	199.68	85	119	0.49
27	780	1	5	230	24	224.74	84	114	0.53

3.1. Materials and experimental details

3.1.1. Alloy studied

The commercial base alloy that is used in the present investigation is Al-$Si_{9.8}$-$Cu_{3.4}$. The chemical composition of the base alloy is shown in Table 2. Investigations are carried out with and without the addition of the new grain refiner and alloying element, the motive being to enhance the mechanical properties of the base alloy.

3.1.2. Master alloy preparation

Al-3.5FeNb-1.5C master alloy for grain refinement has been fabricated by an inoculation technique employing the melting furnace. Aluminum (99.9% pure) ingot, activated carbon powder (~150 μm), and ferroniobium (60% Nb) metals were used as raw materials. Initially, 1 kg of aluminum ingot was melted in a graphite crucible at 900°C and held for 1 h. Then, the preheated activated carbon powder, which was wrapped in an aluminum foil, was added to the molten metal at 1.7 wt.% of C, and after 4–5 min, 7.7 wt.% of ferroniobium (FeNb) metal was added to the melt. The melt temperature was increased up to 1,500°C and held for 6–7 min to promote the dissolution of Nb into Al. This molten metal was poured into a metallic die and allowed to solidify. The solidified Al-3.5FeNb-1.5C grain refiner was then used to conduct grain refinement investigation on pure aluminum and Al-Si cast alloys.

3.1.3. Manufacturing and characterization

The Al-$Si_{9.8}$-$Cu_{3.4}$ alloy, which was in the ingot form, was cut into small pieces to facilitate accommodation in the crucible, and then melted in the induction electric resistance furnace; then it was heated to 800°C till the entire alloy in the crucible melted in an argon atmosphere. The slag formed on the surface of the melt was carefully removed, and preheated graphite-coated stirrer was carefully placed below the surface of the melt to carry out the stirring process to ensure homogenization of the temperature within the melt. Then the melt was then taken into a treatment ladle, and the corresponding predetermined amounts of FeNb-C in the form of the Al–3.5FeNb–1.5C master alloy and Al–6Ni (Al–6 wt.% Ni) were added to the mix and then poured into a pouring hole of the HPDC machine according to the detailed proportion of each casting, as shown in Table 3. After the die casting experimentation process, the cast part was taken from the permanent die. Similarly, experimental cast samples in two sets were obtained using the HPDC method [27], as shown in Figure 1A.

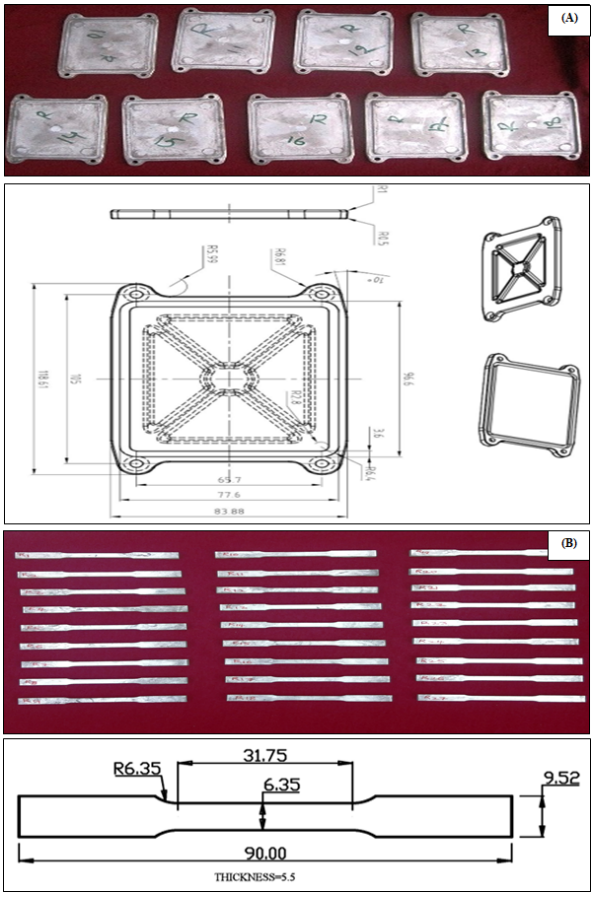


Fig. 1. Sample specimen of HPDC casting **(A)** Final castings with their dimensions **(B)** Tensile specimens with their dimensions used for the experimentations. HPDC, High pressure die casting

The cast samples sized 15 mm × 15 mm × 6 mm were cut for a metallographic investigation using the standard grinding method with SiC sandpapers at 120–1,200 grading, and polished with emery polishing papers (grade from 1/0 to 4/0); and finally, disc polishing was carried out with Al_2O_3 solution using a polishing machine. Further, Tucker's solution (15 mL HNO_3 + 15 mL HF +

45 mL HCL + 25 mL H_2O) was used for etching the polished surfaces to carry out the microstructural examination. Vickers hardness tester (as per ASTME-384 standard) has been used to measure the microhardness values and Brinell hardness values have been taken from Vickers cum Brinell hardness tester performed at 250 kg. For hardness results, an average of two values from each sample of two sets was derived. All the average values obtained using Brinell, as well as the microhardness values, are depicted in Table 3. To evaluate the tensile strength properties of the experimental casting, the rectangular specimens were prepared according to ASTM: B557M-15 standard using the CNC wire cutting machine, as indicated in Figure 1B. All of the ultimate tensile strength (UTS) values were obtained directly from the resolved program of the universal testing machine and tensile values, i.e., the average of two sample values (each from each set), are shown in Table 3. The microstructure and the extracted intermetallic particles of the Al-3.5FeNb-1.5C master alloy were examined by X-ray diffraction (XRD) and FE-SEM.

3.1.4. Density and porosity measurements

The densities of all experimental castings were calculated using the immersion technique. Initially, experimental castings were weighted in air, and then measured while immersed carefully in degassing processed distilled water. Using a Mettler balance, all experimental cast weighings were conducted with accuracy at 0.0001 g.

$$\rho = \frac{w}{(w - w_1)}\rho_w \tag{1}$$

Here "w" shows the weight of the experimental cast part in air, "w_1" shows the weight of the same casting part when it is immersed in processed distilled water, and ""ρ_w is the degassed distilled water density [27].

The density of degassed distilled water at 20°C is 998 kg/m^3. Using the aforesaid method, the densities of the experimental cast parts were measured. The theoretical densities of the castings at different compositions prepared based on experimental design were measured using the rules of mixtures.

Theoretical density is measured by the following equation:

$$\rho_w = \frac{w_1 + w_2 + w_3 + \ldots\ldots + w_n}{\left(\frac{w_1}{\rho_1} + \frac{w_2}{\rho_2} + \frac{w_3}{\rho_3} + \ldots\ldots + \frac{w_n}{\rho_n}\right)} \tag{2}$$

where w_1, w_2, w_3, …, w_n, are weight percentages of the elements and $\rho_1, \rho_2, \rho_3, \ldots, \rho_n$ are the weight densities of the elements. % Porosity has been calculated from theoretical and experimental density values using the following equation, and the resultant values are all depicted in Table 3:

$$\%\text{Porosity} = \frac{(\text{Theoritical density} - \text{Experimental density})}{\text{Theoritical density}} \times 100 \tag{3}$$

3.2. Steps involved in GRA

In 1982, GRA, which is part of the grey system, was introduced by Dr. Deng, as a decision-making approach for multi-criteria, i.e., it converts multi-outcomes (responses) into a single outcome problem [28]. Identification of the optimal solution is based on the grey relational grade (GRG) system because it shows the overall performance of experimental runs [29]. GRA involves the following procedural steps to change the multi-objective optimization problem into a single problem using GRG.

Step 1: Normalized output quality characteristics are computed by the following equation, which allows normalization of the "higher-the-better" quality characteristic:

$$x_i^*(k) = \frac{y_i(k) - \min y_i(k)}{\max y_i(k) - \min y_i(k)} \tag{4}$$

where $x_i^*(r)$ shows normalized data and $y_i(k)$ shows the discerned data for ith experiment by means of the kth response.

Step 2: The following equation is used to obtain the grey relational coefficient (GRC) values to express the mutual relationship between actual and ideal normalized experimental results:

$$\xi_i(k) = \frac{\Delta_{\min} + \xi\Delta_{\max}}{\Delta_i(k) + \xi\Delta_{\max}} \tag{5}$$

where ξ is the distinguishing or identification coefficient, which is normally lies between 0 and 1 and is used mainly to compress or expand the range of GRC values. Normally, the value of ξ is taken as 0.5. Δ_{min} is the global minimum value of $\Delta_i(k)$, and Δ_{max} is the global maximum value of $\Delta_i(k)$, here $\Delta_i(k) = |x_i^*(k) - x_i^o(k)|$

Step 3: In the third step, the GRG values are computed by the following equation:

$$\gamma_i = \frac{1}{n}\sum_{k=1}^{n} \xi_i(k) \tag{6}$$

where γ_i is a GRG value, and n shows the number of output responses.

3.3. Multi-objective optimization by TOPSIS

TOPSIS is a very easy and potent multi-objective decision analyzing method, and helps to carry out optimum single objective solutions among a large number of multi-objective alternate solutions. The basic principle of this method is to determine the optimum solution, which is the shortest distance to a positive ideal solution (PIS) and far from a negative ideal solution (NIS). TOPSIS analytical method is carried out in the following stages.

Stage I: In this stage, the primary decision matrix that has attributes and alternatives is constructed from all the collected data gathered from experimental runs. The decision matrix consists of n attributes and m alternative solutions. In the present process, the output responses are attributes (m) and the experimental trials are alternative solutions (n).

$$D_m = \begin{bmatrix} b_{11} & b_{12} & b_{13} & \cdots & \cdots & b_{1n} \\ b_{21} & b_{22} & b_{23} & \cdots & \cdots & b_{2n} \\ \vdots & \vdots & \vdots & \vdots & \vdots & \vdots \\ b_{m1} & b_{m2} & b_{m3} & \cdots & \cdots & b_{mn} \end{bmatrix} \tag{7}$$

Stage II: Alternative data have been normalized using the following vector normalization method:

$$\mathrm{R}_{ij} = \frac{b_{ij}}{\sqrt{\sum_{i=1}^{m} b_{ij}^2}} \tag{8}$$

where R_{ij} shows a normalized value, corresponding to experiment run i with output response j.

Stage III: A decision matrix is obtained by multiplying each assigned weight of each attribute with the corresponding normalized value. For this study, three output responses were considered and all are having equal importance. So, the assigned weight value equals 1/3, and the weighted normalization for all responses are carried out by following Eq. (6).

$$\begin{aligned} T_{ij} &= R_{ij} W_j \\ \textstyle\sum_{j=1}^{n} W_j &= 1 \end{aligned} \tag{9}$$

Stage IV: Determination of PIS and NIS

PIS and NIS will be determined as

$$\begin{aligned} V^+ &= \left(V_1^+, V_2^+ \ldots V_n^+\right) \\ &= \left\{(\max V_{ij}/j \in B_1), \right. \\ &\quad \left. (\min V_{ij}/j \in B_2, i = 1,2,\ldots n)\right\} \end{aligned} \tag{10}$$

$$\begin{aligned} V^- &= \left(V_1^-, V_2^- \ldots V_n^-\right) \\ &= \left\{(\min V_{ij}/j \in B_1), \right. \\ &\quad \left. (\max V_{ij}/j \in B_2, i = 1,2,\ldots n)\right\} \end{aligned} \tag{11}$$

Here, B_1 is the beneficial set of attributes and B_2 is the non-beneficial set of attributes.

Stage V: Calculation of separation measures of each alternative, i.e., positive separation measures of alternatives from PIS and negative separation measures of alternatives from NIS, are carried out using the following equations.

$$S_i^+ = \sqrt{\sum_{j=1}^{n} (T_{ij} - V^+)^2} \tag{12}$$

$$S_i^- = \sqrt{\sum_{j=1}^{n} (T_{ij} - V^-)^2} \tag{13}$$

where $i = 1, 2, \ldots, m$.

Stage VI: Assessment of closeness coefficient (CC)

In this stage, the CC of every alternative is assessed by Eq. (14). The CC values of every alternative to the ideal solution are computed using Eq. (11).

$$CC = \frac{S_i^-}{S_i^+ + S_i^-} \tag{14}$$

4. Results and discussion

4.1. Microstructure of Al-3.5FeNb-1.5C master alloy

Figure 2A shows the XRD results of the Al-3.5FeNb-1.5C master alloy as a grain refiner. It was observed that the Al-3.5FeNb-1.5C grain refiner primarily contains the α-Al, Al_3Nb, and NbC phases. The intermetallic particles such as Al_3Nb (characterized by a tetragonal structure with lattice parameters a = 3.848 Å and c = 8.615 Å) and NbC (characterized by a face-centered cubic structure with lattice parameter a = 4.430 Å) act as potential nucleation sites for improving the equiaxed structure. Also, the diffraction peak of Fe_2Nb, which is effective in strengthening grain boundaries and suppressing deformation, was detected in the XRD patterns. From Figure 3B, it can be observed that the intermetallic particles (Al_3Nb and NbC) are scattered uniformly and detached from each other; and the sizes of the particles are varied.

4.2. Effect of Al-3.5FeNb-1.5C master alloy on Al-$Si_{9.8}$-$Cu_{3.4}$ base alloy

The microstructures of the commercial Al-$Si_{9.8}$-$Cu_{3.4}$ base alloy with and without the addition of Al-3.5FeNb-1.5C master alloy at 720°C, 750°C, and 780°C are shown in Figure 3. Figures 3A–3C show the microstructures of the Al-$Si_{9.8}$-$Cu_{3.4}$ alloy without the addition of grain refiner, and reveal the coarseness of the grain structures, because their average grain sizes are approximately 61.22 ± 3 μm, 71.93 ± 3 μm, and 64.03 ± 3 μm, respectively. From Figures 3D, 3E, and 3F, it can be observed that the coarse grains of the base alloy are refined to small equiaxed ones by the addition of the Al-3.5FeNb-1.5C grain refiner. Primarily when the base alloy is inoculated with the 0.1 wt.% of Al-3.5FeNb-1.5C grain refiner, very fine grains of the base alloy have been observed, together with uniformity in grains and more number of grains per unit area. From Figure 3D, it can be observed that the average grain size of α-Al of the base alloy was significantly decreased to 22.9 ± 3 μm particularly when the base metal was inoculated with the 0.1 wt.% of Al-3.5FeNb-1.5C grain refiner at 720°C. Also, it was noticed that these grain structures (Figure 4D) are much finer than those grain structures which were refined by the 1.0 wt.% of Al-3.5FeNb-1.5C master alloy. From observing these microstructures, it was understood that the coarse grains become the finest resultant to adding the Al-3.5FeNb-1.5C grain refiner to the base alloy up to a level of 0.1 wt.%. Nevertheless, consequent to the further increase in the addition level of Al-3.5FeNb-1.5C grain refiner from 0.1 wt.% to 1.0 wt.% to the base alloy, the fine grain structure again became coarse, and this can be attributed to the formation of β-Al_5FeSi platelets, which cause the formation of coarse grains. According to the conclusions given by Zedan and

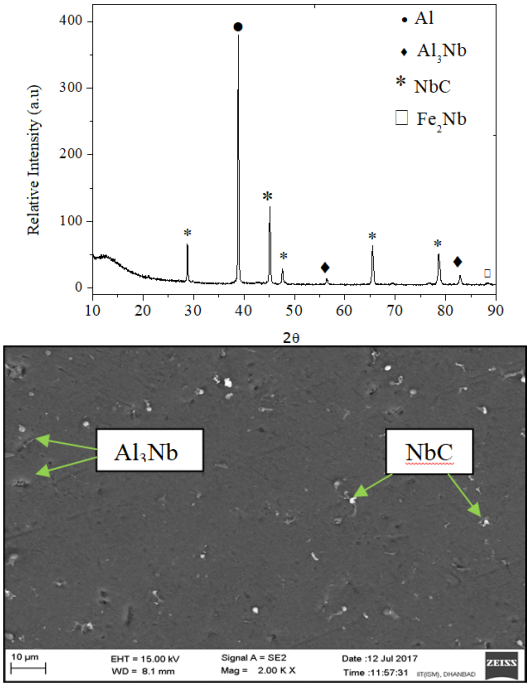


Fig. 2. **(A)** XRD results of the Al-3.5FeNb-1.5C master alloy; **(B)** SEM microstructure of dispersed intermetallic particles extracted from Al-3.5FeNb-1.5C master alloy. XRD, X-ray diffraction

Samuel [30, 31], "these β platelets often result in the formation of large shrinkage cavities due to the inability of the liquid metal to fill the space between the branched platelets". Samuel et al. concluded that the size of β-Al_5FeSi platelets and their distribution are greatly affected by the amount of iron. So, at 1.0 wt.% of Al-3.5FeNb-1.5C grain refiner addition to base alloy, the formation of β-Al_5FeSi platelets has taken place due to increase in the amount of iron content. Based on comparison of the grain size of the alloy with and without grain refinement, as shown in Figure 3, it was observed that the Al-3.5FeNb-1.5C master alloy has a much better grain refining performance particularly at 0.1 wt.% addition to Al-$Si_{9.8}$-$Cu_{3.4}$ alloy. Based on these results, it can be concluded that the developed Al-3.5FeNb-1.5C grain refiner can efficiently refine binary Al-Si alloys due to the formation of niobium silicides, which are more stable than titanium silicides, thus significantly limiting the so-

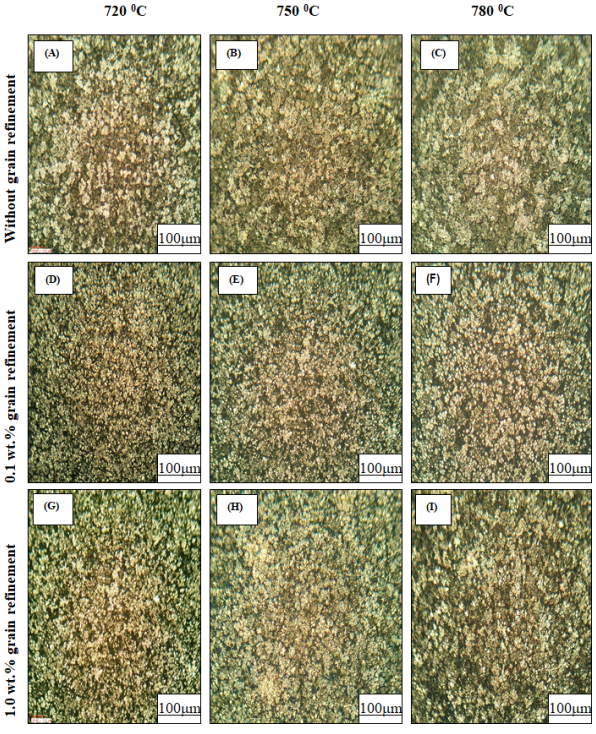


Fig. 3. Optical microscopic images of experimental castings at 720°C, 750°C, and 780°C: **(A–C)** without grain refiner, **(D–F)** 0.1 wt% of Al-3.5FeNb-1.5C, **(G–I)** 1.0 wt% of Al-3.5FeNb-1.5C

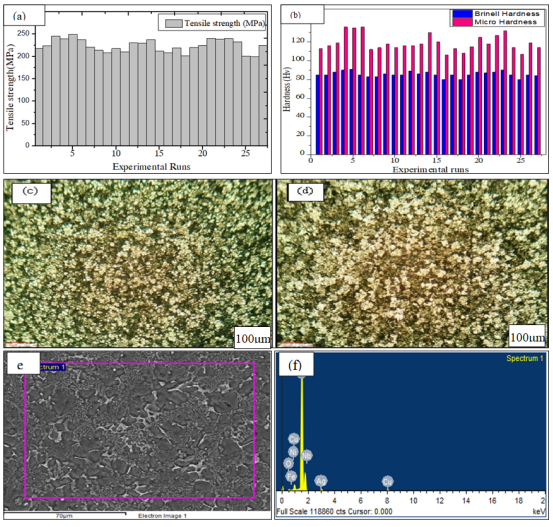


Fig. 4. **(A)** Tensile strength values **(B)** Brinell hardness and microhardness values obtained from experimental runs. **(C)** and **(D)** show the optical microscope images of **(C)** R_5 and **(D)** R_{25} experimental castings, which have the highest and lowest mechanical properties, respectively. **(E)** and **(F)** show the SEM and EDS images of R_5, respectively

called poisoning effect.

4.3. Mechanical properties of die casting Al-$Si_{9.8}$-$Cu_{3.4}$ alloy

Table 3 shows the output characteristics, such as tensile properties and Brinell and microhardness values, which are obtained from the 27 experimental high pressure die casts prepared in two sets at different weight percentages of Al-3.5FeNb-1.5C and Al-6Ni master alloys according to the experimental design. We observe significant effects of grain refinement on the mechanical properties of the commercial Al-$Si_{9.8}$-$Cu_{3.4}$ alloy, and changes are noticeable primarily in UTS and hardness values (Brinell and micro). Specifically, the UTS and hardness values of the Al-$Si_{9.8}$-$Cu_{3.4}$ alloy are improved pursuant to addition of the new grain refiner.

It also can be observed that the grain refinement of the commercial Al-$Si_{9.8}$-$Cu_{3.4}$ alloy utilizing the FeNb-C novel grain refiner leads to a significant improvement in the UTS and hardness measurements, as shown in the experimental runs

Table 4. Normalized data and deviation sequence values of the following characteristics

Run	Deviation Sequences (Δ_{0i})			GRC			GRG	Rank
	Tensile strength	Brinell hardness	Microhardness	Tensile strength	Brinell hardness	Microhardness		
1	0.62	0.55	0.77	0.45	0.48	0.39	0.44	20
2	0.47	0.55	0.67	0.49	0.48	0.43	0.47	13
3	0.07	0.27	0.57	0.87	0.65	0.47	0.66	6
4	0.19	0.09	0.00	0.73	0.85	1.00	0.86	2
5	0.00	0.00	0.03	1.00	1.00	0.94	0.98	1
6	0.24	0.55	0.00	0.68	0.48	1.00	0.72	4
7	0.58	0.73	0.80	0.46	0.41	0.38	0.42	23
8	0.69	0.73	0.73	0.42	0.41	0.41	0.41	24
9	0.82	0.45	0.60	0.38	0.52	0.45	0.45	15
10	0.63	0.55	0.73	0.44	0.48	0.41	0.44	18
11	0.51	0.55	0.67	0.39	0.48	0.43	0.43	21
12	0.38	0.18	0.67	0.57	0.73	0.43	0.58	9
13	0.38	0.45	0.60	0.57	0.52	0.45	0.52	11
14	0.24	0.27	0.20	0.68	0.65	0.71	0.68	5
15	0.74	0.55	0.53	0.40	0.48	0.48	0.46	14
16	0.83	1.00	1.00	0.38	0.33	0.33	0.35	25
17	0.61	0.55	0.77	0.45	0.48	0.39	0.44	19
18	0.97	1.00	0.93	0.34	0.33	0.35	0.34	26
19	0.59	0.55	0.70	0.46	0.48	0.42	0.45	16
20	0.49	0.27	0.37	0.50	0.65	0.58	0.58	10
21	0.17	0.36	0.60	0.74	0.58	0.45	0.59	8
22	0.22	0.27	0.30	0.70	0.65	0.63	0.66	7
23	0.18	0.09	0.13	0.73	0.85	0.79	0.79	3
24	0.33	0.55	0.73	0.60	0.48	0.41	0.49	12
25	0.99	1.00	0.97	0.34	0.33	0.34	0.34	27
26	1.00	0.55	0.57	0.33	0.48	0.47	0.43	22
27	0.49	0.64	0.73	0.50	0.44	0.41	0.45	17

GRC, Grey relational coefficient; GRG, Grey relational grade.

R_4 and R_{22}. Moreover, these properties (UTS and hardness) of the Al-$Si_{9.8}$-$Cu_{3.4}$ alloy are further increased due to addition of Al-6Ni master alloy, particularly at 0.1 wt.% of Al-3.5FeNb-1.5C and 0.5 wt.% of Al-6Ni master alloys, as observed in the experimental runs R_5 and R_{25}.

Quantitatively, the UTS of the unrefined Al-$Si_{9.8}$-$Cu_{3.4}$ alloy is about 218.39 $\pm$ 3 MPa, and after the addition of 0.1 wt.% of Al-3.5FeNb-1.5C and 0.5 wt.% of Al-6Ni master alloys, the UTS is increased to 249.08 $\pm$ 3 MPa. That is to say, the average value of the UTS is increased by 12.3%. The hardness values (Brinell and micro) of the Al-$Si_{9.8}$-$Cu_{3.4}$ are also increased from 85 $\pm$ 3 Hv to 91 $\pm$ 3 Hv and from 113 $\pm$ 3 Hv to 136 $\pm$ 3 Hv owing to the addition of these two master alloys, respectively. The UTS and macro- and microhardness values for all experimental runs are shown in Figures 4A and 4B. It is apparent that the average hardness (Brinell and micro) and UTS values of sample R_5, having a porosity percent of less than 0.3%, are more than 90 Hv for Brinell hardness, 135 $\pm$ 3 Hv for microhardness, and 249.08 $\pm$ 3 MPa for UTS. It is worth noticing that the samples with 0.1 wt.% of Al-3.5FeNb-1.5C and 0.5 wt.% of Al-6Ni master alloys' addition possess the highest UTS and hardness. But they have deteriorated when the addition of 1.0 wt.% of Al-3.5FeNb-1.5C compared with base metal, quantitatively the lowest UTS and hardness values at experimental run R_{25} are 200.27 $\pm$ 3 MPa, 80 $\pm$ 3 Hv, and 107 $\pm$ 3 Hv because its microstructure is much

larger than other samples such as R_4 and R_5 as shown in Figures 4C and 4D.

4.4. Grey relational coefficients (GRG)

The investigation aims to enhance the process improvement and strength of aluminum cast alloys, and thus all the output characteristics such as macro- and microhardness and tensile strength are to be maximized. The output characteristics were normalized for "higher-the-better" using Eq. (1). Table 4 expresses the normalized value of an experimental result, GRC, and GRG calculated through Eqs (1) and (3). The GRCs and overall GRG for each combination are depicted in Table 4.

For every outcome response, the "higher-the-better" condition is chosen. It is always desirable to get the highest value of the GRG. The higher GRG grade indicates a closeness to the optimal response in the process. It is noticed that experiment run 5 has the highest GRG of 0.98. The average optimal values of GRG for each parameter at levels 1–3 are given in Table 5 and plotted in Figures 5A and 5E. The main effects of the various parameters, when changed from the lower to a higher level, are also given in Table 5.

From Figure 4, we can ascertain that the parameter B is more prominent than other parameters; also, it is clear that average GRG appears to be maximum at the second level of the parameters B and C, at the first level of the parameters A and D, and then at the third level of the parameter E – i.e., A_1, B_2, C_2, D_1, and E_3 can be recognized as the best levels for enhancing the mechanical properties of the high pressure die casts of Al-$Si_{9.8}$-$Cu_{3.4}$ aluminum alloy. From GRA, the experiment run, which has the highest grey relational grade, i.e. which is very close to one is considered as an optimal solution. As per Table 5, experimental run No. 5 has the highest GRG of 0.98, and corresponding output response values are considered as optimal values would get at optimal levels (A_1, B_2, C_2, D_1, and E_3) of the process parameters.

4.5. TOPSIS

The normalization, weighted normalization, separation, and their relative CC values, which were computed by Eqs (7) and (14), are depicted in Table 6. The experimental run that has the highest CC value, i.e., a value that is very close to 1, is considered the best experimental run. As per the values of CC, which are shown in Table 6, experimental run 5 has the highest CC value of 0.972. The ranks, which are prepared as per the grade (higher to lower) of CC values of experimental runs, are shown as:

$$5 > 4 > 23 > 6 > 14 > 22 > 3 > 20 > 21 > 12 > 13 > 24 > 2 > 15 > 27 > 19 > 9 > 17 > 10 > 1 > 21 > 26 > 7 > 8 > 16 > 18 > 25.$$

Based on the ranking order of experimental runs, it could be understood that experimental run 5, which has the highest CC value of 0.972, is the best optimum solution and that experimental run 4 is the next optimum solution, being the first to follow experimental run 5. Also, it was identified that the experimental run 25 is the worst optimum solution among all alternatives. To obtain an optimized set of process parameters from the TOPSIS methodology, the average values of CC for each parameter at levels 1–3 are given in Table 7 and plotted in Figures 6A and 6E. The main effects of the various parameters, when changed from the lower to a higher level, are also given in Table 7. From Figure 6, it is known that the parameter B is more prominent than other parameters, also it is clear that average CC appears to be maximum at the second level of the parameters B and C, at the first level of parameters A and D and the at the third level of parameter E. i.e., A_1, B_2, C_2, D_1 and E_3 as the best levels for enhancing the mechanical properties of the high pressure die casts of Al-$Si_{9.8}$-$Cu_{3.4}$ aluminum alloy that are a molten metal temperature of 120°C, 0.1 wt.% of Al-3.5FeNb-1.5C grain refiner, 0.5 wt.% of Al-6Ni alloying addition, die temperature of 230°C and injection pressure of 24 MPa.

4.6. Comparison of GRA and TOPSIS results and confirmation test results

The optimum results which are obtained from GRA and TOPSIS multi optimized analytical techniques are compared and noticed that both have the same set of combination of process parameters i.e

Table 5. Mean values of GRG at different levels and their main effects

Parameter destination	Input parameters	Level 1	Level 2	Level 3	Max/min
A	Molten metal temperature (°C)	0.601	0.470	0.530	0.131
B	Al-3.5FeNb-1.5C (wt%)	0.516	0.683	0.403	0.280
C	Al-6Ni (wt%)	0.496	0.578	0.527	0.082
D	Die temperature (°C)	0.539	0.537	0.525	0.015
E	Injection pressure (MPa)	0.508	0.528	0.565	0.056

GRG, grey relational grade.

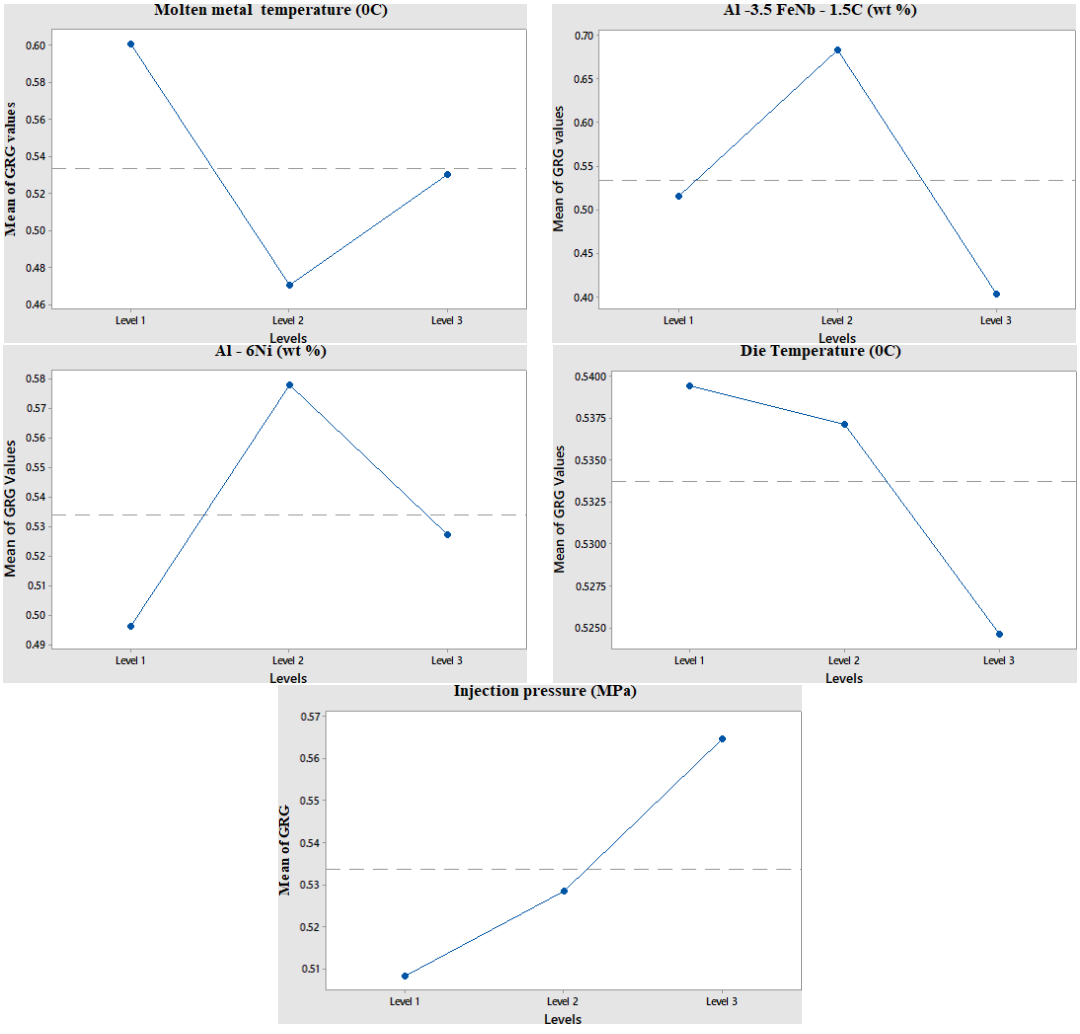


Fig. 5. Effect of process parameters on GRG. GRA, grey relational analysis

A_1, B_2, C_2, D_1, E_3 as an optimum result. The comparison graph between the grade values of GRG and CC concerning the sequence of experimental runs is shown in Figure 7. From this graph, it is noticed that the same similarity has been followed in both the techniques, except for experiments 4, 14, and 20. Also, it is observed that experimental run 5 has the highest grade value and that experimental run 25 has the lowest grade value. Therefore, the confirmation test was performed to validate the predicted CC and grey grade values using the fol-

Table 6. TOPSIS results

Expt. runs	Normalization			Weighted normalization			Separation		CC
	Tensile strength	Brinell hardness	Vickers hardness	Tensile	Brinell	Vickers	S^-	S^+	
1	0.187	0.191	0.183	0.062	0.064	0.061	0.016	0.008	0.324
2	0.192	0.191	0.188	0.064	0.064	0.063	0.014	0.010	0.416
3	0.211	0.198	0.192	0.070	0.066	0.064	0.010	0.016	0.628
4	0.206	0.202	0.220	0.069	0.067	0.073	0.003	0.021	0.886
5	0.214	0.204	0.218	0.071	0.068	0.073	0.001	0.023	0.972
6	0.204	0.191	0.220	0.068	0.064	0.073	0.005	0.020	0.786
7	0.189	0.187	0.181	0.063	0.062	0.060	0.016	0.007	0.306
8	0.184	0.187	0.184	0.061	0.062	0.061	0.017	0.007	0.283
9	0.179	0.193	0.191	0.060	0.064	0.064	0.016	0.008	0.350
10	0.187	0.191	0.184	0.062	0.064	0.061	0.016	0.008	0.333
11	0.181	0.191	0.188	0.060	0.064	0.063	0.016	0.008	0.321
12	0.198	0.200	0.188	0.066	0.067	0.063	0.012	0.013	0.511
13	0.197	0.193	0.191	0.066	0.064	0.064	0.012	0.012	0.500
14	0.204	0.198	0.210	0.068	0.066	0.070	0.005	0.018	0.779
15	0.182	0.191	0.194	0.061	0.064	0.065	0.014	0.009	0.391
16	0.179	0.180	0.171	0.060	0.060	0.057	0.022	0.003	0.110
17	0.188	0.191	0.183	0.063	0.064	0.061	0.016	0.008	0.334
18	0.172	0.180	0.175	0.057	0.060	0.058	0.022	0.001	0.059
19	0.189	0.191	0.186	0.063	0.064	0.062	0.015	0.009	0.370
20	0.193	0.198	0.202	0.064	0.066	0.067	0.009	0.014	0.598
21	0.206	0.196	0.191	0.069	0.065	0.064	0.010	0.014	0.582
22	0.204	0.198	0.205	0.068	0.066	0.068	0.006	0.017	0.727
23	0.206	0.202	0.213	0.069	0.067	0.071	0.004	0.020	0.845
24	0.200	0.191	0.184	0.067	0.064	0.061	0.014	0.011	0.452
25	0.172	0.180	0.173	0.057	0.060	0.058	0.022	0.001	0.032
26	0.171	0.191	0.192	0.057	0.064	0.064	0.018	0.008	0.309
27	0.193	0.189	0.184	0.064	0.063	0.061	0.015	0.009	0.380

CC, closeness coefficient.

Table 7. Response table of average values of CC for TOPSIS

Parameter destination	Input parameters	Level 1	Level 2	Level 3	Max/min
A	Molten metal temperature (°C)	**0.550**	0.371	0.478	0.179
B	Al-3.5FeNb-1.5C (wt%)	0.454	**0.704**	0.240	0.464
C	Al-6Ni (wt%)	0.399	**0.540**	0.460	0.141
D	Die temperature (°C)	**0.499**	0.463	0.435	0.036
E	Injection pressure (MPa)	0.4147	0.465	**0.519**	0.104

CC, Closeness coefficient.

lowing relation:

$$\gamma = \gamma_m + \sum_{i=1}^{q} (\overline{\gamma}_i - \gamma_m) \tag{15}$$

where γ_m is total mean of CC/GRG and $\overline{\gamma}_i$ is mean of CC/GRG at an optimal level of parameters.

The predicted value of GRG was 0.809 and CC was 0.948, i.e., the predicted grey grade value of GRA is less than the predicted closeness value of TOPSIS. Similarly, based on the experimental confirmation, the highest values of the grey grade and CC were 0.979 and 0.972, respectively. The results

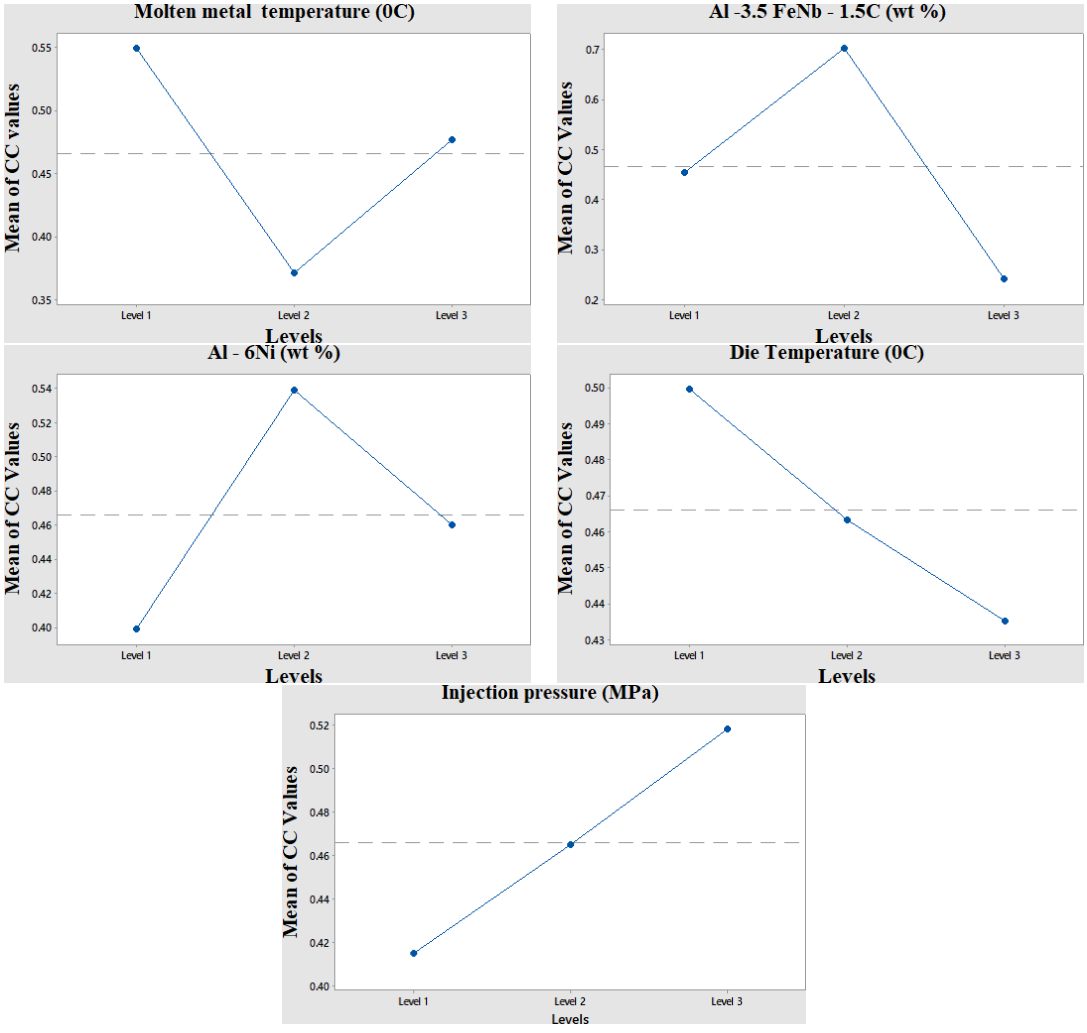


Fig. 6. Effect of process parameters on CC. CC, closeness coefficient

Table 8. Results' comparison at initial and optimal levels by GRA and TOPSIS methods

S. No	Parameter	Initial value	Predicted value	Experimental value
		A_2, B_1, C_1, D_2, E_3	A_1, B_2, C_2, D_1, E_3	A_1, B_2, C_2, D_1, E_3
1	Tensile strength	218.388	–	249.085
2	Brinell hardness	85	–	91
3	Vickers microhardness	113	–	135
4	Grey relational grade	0.4396	0.8087	0.9792
5	Closeness coefficient	0.3242	0.9481	0.9715
6	Improvement of GRG	–	0.5396	–
7	Improvement of CC	-	0.6473	–

CC, closeness coefficient; GRA, grey relational analysis; GRG, grey relational grade.

of confirmation are depicted in Table 8. Mainly, a significant improvement has been observed in grey grade value from the initial set of parameters to an optimal set of parameters combination was 0.540 and CC was 0.647. Further, it was observed that optimal process parameters' combination results

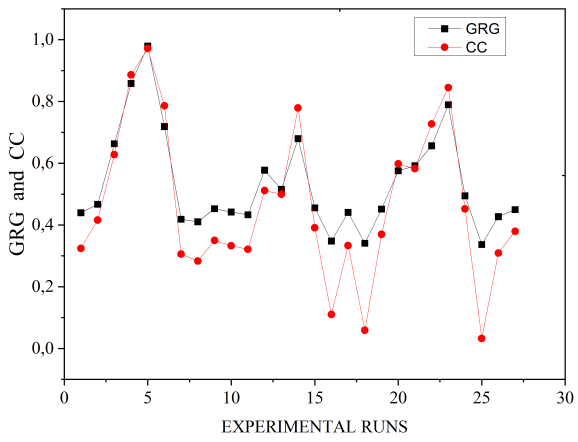


Fig. 7. GRG and CC value of each experimental run. CC, closeness coefficient; GRG, Grey relational grade

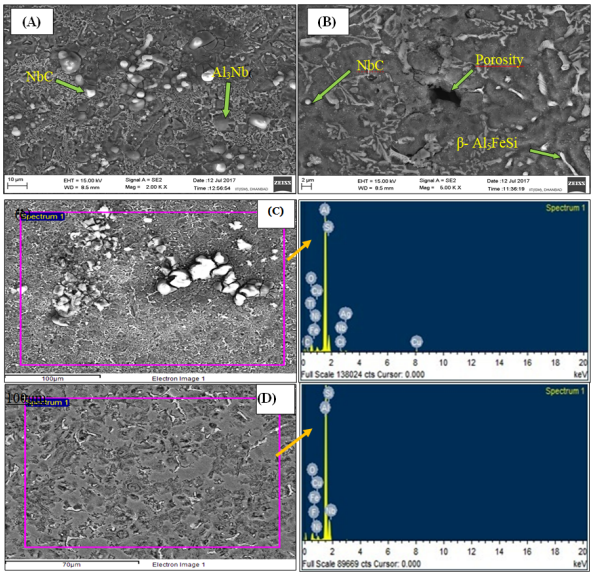


Fig. 8. SEM images of Al-$Si_{9.8}$-$Cu_{3.4}$ alloy: Experimental runs of **(A)** $\boldsymbol{R_5}$ at 0.1 wt.% of Al3.5FeNb-1.5C and 0.5 wt.% of Al-6Ni with base alloy and **(B)** $\boldsymbol{R_{25}}$ at 1.0 wt.% of Al3.5FeNb-1.5C with base alloy; EDX pattern of **(C)** Experimental run $\boldsymbol{R_5}$ and **(D)** Experimental run $\boldsymbol{R_{25}}$

yield a CC value higher than the seventh experiment for the TOPSIS approach and higher than the 10th experiment in the GRA approach, which is the highest value in the L27 orthogonal array of the set of experiments.

4.7. Metallurgical characterization of the die castings at highest and least values of results

SEM images with EDX examination of the experimental runs R_5 at 0.1 wt.% of Al-3.5FeNb-1.5C and 0.5 wt.% of Al-6Ni with base alloy and R_{25} at 1.0 wt.% of Al-3.5FeNb-1.5C with base alloy are shown in Figures 8A and 8D, respectively. It is observed that mainly three prominent elements (Al, Nb, and C) react to structure various types of compounds those are niobium aluminides (Al_3Nb) and niobium carbides (NbC), which act as potential heterogeneous nucleation sites i.e., inoculants which promote the effective grain refinement of Al-Si alloys through heterogeneous nucleation. Nevertheless, from Figure 8B it can be observed that the β-Al_5FeSi platelets have appeared along with Al_3Nb and NbC. These platelets often result in the formation of large shrinkage cavities due to the inability of the liquid metal to penetrate the spaces between the branched platelets. The improvement of UTS and hardness properties has been observed in experimental run R_5, as shown in Figure 8A, via effective grain refinement by Al_3Nb and NbC in the heterogeneous nucleation sites. However, the porosity has been increased in the experimental run R_{25}, as shown in Figure 8B, because of β-Al_5FeSi platelets that cause the formation of large shrinkage cavities. It was observed from the EDX pattern, as shown in Figures 8C and 8D, that presence of the elements Al, Si, Cu, Fe, Nb, C, and Ni in base Al-$Si_{9.8}$-$Cu_{3.4}$ alloy confirms the distribution of FeNb, C, and Ni materials. The fracture morphologies of the experimental runs R_5 and R_{25}, shown in Figures 9A and 9B, indicate that the specimen has the highest and lowest GRG and CC values. The effect of grain refiner content in the base materials on the fracture morphology of the tensile tested samples was examined to understand in a better way the tensile strength mechanism. It is clearly observed from Figure 9A that the fracture patterns are composed of smaller cleavage planes and a few small dimples. In the materials (experimental run R_5), the size of the voids is decreased with the addition of 0.1 wt.% of Al-3.5FeNb-1.5C and 0.5 wt.% of Al-6Ni content in the Al-$Si_{9.8}$-$Cu_{3.4}$ alloy. The

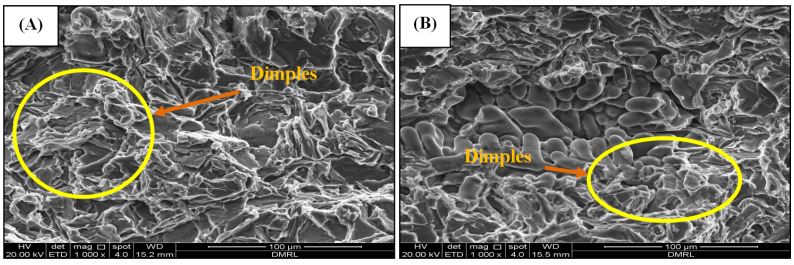


Fig. 9. SEM images of fracture pattern of experimental runs of **(A)** $\boldsymbol{R}_5$ at 0.1 wt.% of Al3.5FeNb-1.5C and 0.5 wt.% of Al-6Ni with base alloy and **(B)** $\boldsymbol{R}_{25}$ at 1.0 wt.% of Al3.5FeNb-1.5C with base alloy

grain refinement in the material causes the voids' sizes to shrink. And it is observed from Figure 9B that uniformly distributed and bigger sized voids are present in the fracture morphology. It may be that the fracture morphology of Al-$Si_{9.8}$-$Cu_{3.4}$ alloy with the addition of 1.0 wt.% of the Al-3.5FeNb-1.5C master alloy revealed a typical ductile fracture characteristic, consisting of numerous dimples over the entire surface. The strength of Figure 9A is higher than that of Figure 9B, and this is due to grain refinement. lower size of dimples noticed in Figure 9A reveals that grain refinement and to detach the grain boundary need more load, the results of grain refinement that have more grain boundaries.

5. Conclusions

The microstructural and mechanical properties of commercial Al-$Si_{9.8}$-$Cu_{3.4}$ alloy die castings influenced by grain refiner and alloying additions have been investigated successfully. During this investigation, the TOPSIS methodology along with GRA for optimization of the die casting process for the fabrication of aluminum-silicon alloy casts has been implemented. The following summarized conclusions can arrived at based on the experimental investigations:

1. Appreciable grain refinement of Al-$Si_{9.8}$-$Cu_{3.4}$ alloy has been observed, particularly at lower level of addition of 0.1 wt.% of Al-3.5FeNb-1.5C; conversely, poor grain refining efficiency was observed at a higher level of addition of 1.0 wt.% of Al-3.5FeNb-1.5C, which results in the agglomeration of NbC and formation of β-Al_5FeSi platelets.
2. The developed Al–3.5FeNb–1.5C grain refiner conducts a significant performance of grain refinement on the commercial Al-$Si_{9.8}$-$Cu_{3.4}$ alloy die castings due to the inauguration of niobium silicides ($NbSi_2$, Nb_3Si, and Nb_5Si_3), which are more stable than titanium silicides, effectively encountering the so-called poisoning effect as a result. So, the mechanical properties of the Al-$Si_{9.8}$-$Cu_{3.4}$ alloy die casting are significantly improved by the addition of the 0.1 wt.% Al-3.5FeNb-1.5C master alloy and Al-6Ni alloy. In quantitative terms, the improvement in mechanical properties can be expressed thus: UTS, Brinell hardness, and microhardness values have been increased by 12.3%, 7.0%, and 20%, respectively. Hence the effective grain refinement performance of the novel Al-3.5FeNb-1.5C mater alloy for Al-Si cast alloys, where silicon content is more than 4 wt.% is accepted and recommended to industries.
3. Both the TOPSIS and GRA have an identical set of optimal parameters' combination, i.e., A_1-B_2-C_2-D_1-E_3, for achieving better mechanical properties and microstructure. The confirmation test results reveal an increase in the CC value by 0.647 and in the grey grade value by 0.540.

References

[1] Camicia G, Timelli G. Grain refinement of gravity die cast secondary $AlSi_7Cu_3Mg$ alloys for automo-

tive cylinder heads. Trans Nonferrous Met Soc China. 2016;26(5):1211–21.

[2] Biswas P, Prasadu KD, Manas Kuma M. Effect of Bi addition on microstructure and mechanical properties of hypereutectic Al-17.6Si alloy. Mater Res Express. 2019;6(11):1–26. https://doi.org/10.1088/2053-1591/ab4d34.

[3] Cai Q, Mendis Ch. L, Chang TH, Fan Z. Microstructure and mechanical properties of new die-cast quaternary Al-Cu-Si-Mg alloys. Mater Sci Eng A. 2021;800.140357. https://doi.org/10.1016/j.msea.2020.140357.

[4] Lu L, Dahle AK. Effects of combined additions of Sr and AlTiB grain refiners in hypoeutectic Al–Si foundry alloys. Mater Sci Eng A. 2006;435(436):288–96.

[5] Kori SA, Auradi V, Murty BS. Poisoning and fading mechanism of grain refinement in Al-7Si alloy. Mater Forum. 2005;29:387–93.

[6] Murty BS, Kori SA, Chakraborty M. Grain refinement of aluminum and its alloys by heterogeneous nucleation and alloying. Int Mater Rev. 2002;47(1):3–29.

[7] Liu F, Zhao H, Yang R, Sun F. Microstructure and mechanical properties of high vacuum die-cast AlSiMgMn alloys at as-cast and T6-treated conditions. Materials (Basel). 2019;12(13):2065. https://doi.org/10.3390/ma12132065.

[8] Chen Z, Wang T, Gao L, Fu H, Li T. Grain refinement and tensile properties improvement of aluminum foundry alloys by inoculation with Al–B master alloy. Mater Sci Eng A. 2012;553:32–6.

[9] Sigsworth GK. The grain refining of aluminum and phase relationships in the Al–Ti–B system. Metall Mater Trans A. 1984;15:277–82.

[10] Guzowski MM, Sigworth GK, Sentner DA. The role of boron in the grain refinement of aluminum with titanium. Metall Mater Trans A. 1987;18:603–19.

[11] Auradi V, Kori SA. Reaction time for the manufacturing of Al–Ti–B (Ti:B = 5:1, 1:3) master alloys and their grain refining efficiency on Al–7Si alloys. Trans Indian Inst Met. 2012;65:637–45.

[12] Han YF, Li K, Wang J, Shu D, Sun BD. Microstructure and grain refining performance of Al–5Ti–1B master alloy prepared under high-intensity ultrasound. Mater Sci Eng A. 2006;430:326–31.

[13] Li H, Lin B, Xu R, Liu K, Xiao H, Zhao Y. Enhanced mechanical properties of Al–Si–Cu–Mn–Fe alloys at elevated temperatures through grain refinement and dispersoid strengthening. Mater Sci Technol. 2020;36(3):307–19. https://doi.org/10.1080/02670836.2019.1705039.

[14] Birol Y. Production of Al–Ti–B grain refining master alloys from B_2O_3 and K_2TiF_6. J Alloys Compd. 2007;443:94–8.

[15] Qiu D, Taylor JA, Zhang MX. A mechanism for the poisoning effect of silicon on the grain refinement of Al-Si alloys. Acta Mater. 2007;55:1447–56.

[16] Birol Y. AlB_3 master alloy to grain refine $AlSi_{10}Mg$ and $AlSi_{12}Cu$ aluminium foundry alloys. J Alloys Compd. 2012;513:150–3.

[17] Zhu M, Jian ZY, Yang GC. Effects of T6 heat treatment on the microstructure, tensile properties, and fracture behavior of the modified A356 alloys. Mater Des. 2012;36(1):243–9.

[18] Sritharan T, Li H. Influence of titanium to boron ratio on the ability to grain refine aluminium–silicon alloys. J Mater Process Technol. 1997;63:585–9.

[19] Murty BS, Kori SA, Chakraborty M. Influence of silicon and magnesium on grain refinement in aluminium alloys. Mater Sci Technol. 1999;15:986–92.

[20] Murty BS, Kori SA, Chakraborty M. Development of an efficient grain refiner for Al–7Si alloy and its modification with strontium. Mater Sci Eng A. 2000;283:94–104.

[21] Nowak M, Bolzoni L, Hari Babu N. Grain refinement of Al–Si alloys by Nb–B inoculation. Part I: Concept development and effect on binary alloys. Mater Des. 2015;66:366–75.

[22] Apparao K. Ch, Birru AK. Grain refining potency of Al–3.5FeNb–1.5C master alloy on pure Al and Al-$Si_{9.8}$-$Cu_{3.4}$ alloy. China Foundry J. 2018;15(4):314–9.

[23] Mostafa A, Mohammad HS, Parviz A, Abolfazl K. Hybrid multi-objective optimization of microstructural and mechanical properties of B_4C/A356 composites fabricated by FSP using TOPSIS and modified NSGA-II. Trans Nonferrous Met Soc China. 2017;27:2317–33.

[24] Srinivasan L, Khan Md C, Deepan BKT, Sathiya P, Biju S. Application of GRA and TOPSIS optimization techniques in GTA welding of 15CDV6 aerospace material. Trans Indian Inst Met. 2017;71:373–282.

[25] Sudhagar S, Sakthivel M, Mathew PJ, Daniel A. A multi criteria decision making approach for process improvement in friction stir welding of aluminium alloy. Measurement. 2017;108:1–8.

[26] Apparao K. Ch, Birru AK. QFD-Taguchi based hybrid approach in die casting process optimization. Trans Nonferrous Met Soc China. 2017;27:2345–2356.

[27] Apparao K. Ch, Birru AK, Kumar BP. Porosity formation studies in high pressure die castings of Al-9Si-3Cu alloy based on Taguchi method. Int J Struct Integr. 2021;13(1):78–91.

[28] Deng J. Introduction to grey system. J Grey Syst. 1989;1:1–24.

[29] Ghetiya ND, Patel KM, Kavar AJ. Multi-objective optimization of FSW process parameters of aluminium alloy using taguchi-based grey relational analysis. Trans Indian Inst Met. 2016;69:917–23.

[30] Zedan Y, Samuel FH. Effects of Fe intermetallics on the machinability of heat-treated Al-(7-11)% Si alloys. J Mater Process Technol. 2010;210:245–57.

[31] Samuel AM, Doty HW, Valtierra S, Samuel FH. Beta Al_5FeSi phase platelets-porosity formation relationship in A319.2 type alloys. Int J Met. 2017;12(1):55–70.

Received 2021-10-28
Accepted 2022-05-30